Biomedicine & Pharmacotherapy 166 (2023) 115402

Contents lists available at ScienceDirect

Biomedicine & Pharmacotherapy

journal homepage: www.elsevier.com/locate/biopha

Ferrocene/ β-cyclodextrin based supramolecular nanogels as theranostic systems

Khadijeh Soleimani [a], Siamak Beyranvand [a], Zeinab Souri [a], Zainab Ahmadian [b,*], Abdollah Yari [a], Abbas Faghani [c], Azim Shams [a], Mohsen Adeli [a,*]

[a] Department of Chemistry, Lorestan University, Khorramabad 6815144316, Iran
[b] Department of Pharmaceutics, School of Pharmacy, Lorestan University of Medical Sciences, Khorramabad, Iran
[c] Institut für Chemie und Biochemie, Freie Universität Berlin, Takustr. 3, 14195 Berlin, Germany

ARTICLE INFO

Keywords:
Anticancer
Redox responsive
Supramolecular
Theranostics
Nanogels

ABSTRACT

A supramolecular redox responsive nanogel (NG) with the ability to sense cancer cells and loaded with a releasing therapeutic agent was synthesized using hostguest interactions between polyethylene glycol-grafted-β-cyclodextrin and ferrocene boronic acid. Cyclic voltammetry matched with other spectroscopy and microscopy methods provided strong indications regarding host-guest interactions and formation of the NG. Moreover, the biological properties of the NG were evaluated using fluorescence silencing, confocal laser scanning microscopy, and cell toxicity assays. Nanogel with spherical core-shell architecture and 100–200 nm sized nanoparticles showed high encapsulation efficiency for doxorubicin (DOX) and luminol (LU) as therapeutic and sensing agents. High therapeutic and sensing efficiencies were manifested by complete release of DOX and dramatic quenching of LU fluorescence triggered by 0.05 mM H_2O_2 (as an ROS component). The NGs showed high ROS sensitivity. Taking advantage of a high loading capacity, redox sensitivity, and biocompatibility, the NGs can be used as strong theranostic systems in inflammation-associated diseases.

1. Introduction

Simultaneous detection and treatment of cancer, as one of the main causes of death worldwide, remains a challenging issue [1–4]. Theranostic systems, a combination of diagnostic and therapeutic agents loaded in a nanocarrier, have emerged as an outstanding approach in the field of cancer therapy [5]. Due to their versatility and biocompatibility, supramolecular systems including micelles [6], liposomes [7] and nanocapsules [8] have attracted a great deal of attention for the construction of theranostic systems [9–12]. However, supramolecular systems dissociate to their building blocks upon administration when they cross their critical aggregation concentration. This leads to the unwanted burst release of encapsulated drugs [13,14]. Supramolecular polymer nanogels (PNGs), as three-dimensional networks of physically crosslinked polymer chains, are an alternative to the above-mentioned traditional carriers [15–21]. The higher stability of supramolecular PNGs than that of micelles and liposomes results in a longer circulation time and efficient biodistribution, as well as accumulation of drugs in tumors [17,22,23]. Furthermore, environmentally responsive PNGs, sensitive to external stimuli such as temperature, pH, light, and redox agents, are useful platforms to construct smart theranostic systems [24–31]. Smart PNGs improve the therapeutic efficacy of drugs by preserving their concentration at an effective level, controlling release of payload in targeted tissue, and reducing drug toxicity [32–35]. Among different internal stimuliresponsive systems, redox-responsive counterparts have gained great attention for cancer therapy due to the higher concentration of GSH in cancer tissues [36,37]. Different synthetic pathways have been developed over the years to meet the criteria of tunable size, morphology, physico-chemical properties, controlled drug delivery, and selective cellular uptake. Chemical crosslinking methods, such as polymerization and interfacial reaction, have been increasingly improved to overcome the shortcomings of available formulations with particular attention to biocompatibility issues. On the other hand, physical approaches have been refined to produce NGs showing responsivity to biochemical stimulus. However, the synthesis of effective systems with suitable physicochemical properties and biological activities is a long-standing challenge [38]. Dynamic and reversible host-guest interactions have been employed to prepare a large number

* Corresponding authors.
E-mail addresses: z.ahmadian@arums.ac.ir (Z. Ahmadian), mohadeli@yahoo.com (M. Adeli).

https://doi.org/10.1016/j.biopha.2023.115402
Received 5 July 2023; Received in revised form 24 August 2023; Accepted 28 August 2023
Available online 4 September 2023

of stimuli-responsive supramolecular systems, including nanogels (NGs) [39]. Cyclodextrins (CDs), with a hydrophobic cavity and hydrophilic functional groups, have frequently been used as host molecules for the construction of smart redox-responsive supramolecular systems [40–46]. Following a report regarding the anticancer activity of ferrocene (Fc) by Brynes and co-workers in the late 1970 s, Fc-based compounds have attracted a great deal of attention in the field of cancer therapy [47]. The redox switchable hydrophobicity of Fc-containing polymers makes them attractive candidates for the construction of smart materials, with the ability to release a specific drug at the tumor site upon host-guest interactions [48,49]. In this work, a redox stimuli-responsive NG was synthesized by host-guest interactions between Fc-boronic acid (FcBA) as a guest and polyethylene glycol-grafted-β-cyclodextrin)PEG-g-CD(as *a* host molecule. FcBA played *a* dual role in the formation of NGs, including host-guest interaction and covalent attachment with the cavity and hydroxyl groups of cyclodextrin, respectively. The NG was used as *a* platform to construct *a* theranostic system by encapsulating doxurobicin (DOX) and luminol (LU). DOX as a hydrophilic therapeutic anticancer drug that can decrease or inhibit tumor growth via blocking the topo isomerase 2 enzyme that is required for proliferation and growth of cancer cells [50,51]. Furthermore, luminol, as a common chemiluminescent molecule that can be oxidized by hydrogen peroxide to create an unstable high-energy intermediate, can dissipates energy back to the ground state by emitting photons and thus can be used in direct chemiluminescence for the purpose of detection of cancer cells [52]. Thus, the main goals of the present study were the fabrication of modular redox-responsive NGs through host–guest interaction-directed self-assembly of polymers and loading of DOX and LU for the simultaneous detection and treatment of cancer cells.

2. Materials and methods

2.1. Materials

Ferroceneboronic acid (FcBA), β-cyclodextrin (β-CD), p-toluenesulfonic anhydride, luminal, and doxorubicin (DOX) were purchased from Sigma Aldrich (Germany). HCl, H_2SO_4, H_2O_2, cyanuric chloride, polyethylene glycol (PEG), ethylenediamine, CCK-8 solution, sodium hydroxide, potassium chloride, paraformaldehyde, tetraethyl ammonium tetrafluoroborate, methanol, dichloromethane, diethyl ether, ethanol, dimethyl sulfoxide (DMSO), RPMI 1640, DPBS, fetal bovine serum (FBS), and cyanuric chloride (triazine) were purchased from Merck (Germany). MCF-7 cells were prepared from the Pasteur Institute (Iran). Dialysis membrane tubing (Biotech Cellulose Ester, width: 31 mm, MWCO: 2 kDa) and deionized water were used for the purification of the synthesized materials.

3. Instrumental analysis

IR spectra were recorded using a Bruker-Tensor 320 FT-IR spectrometer after mixing samples with analytical grade KBr at a weight ratio of 5/200 mg. The morphology and structure of the NGs were investigated using an LEO 440i scanning electron microscope (SEM) under vacuum at an operating voltage of 10 kV after coating the dried samples with a thin layer of gold by sputtering for 15 s. A Shimadzu UV–Vis 1650 PC spectrophotometer using a cell with a 1.0 cm path length was used to record the absorption spectra of the systems in aqueous solution. The NMR spectra of the synthesized materials were recorded using a Bruker ECX 400 (400, 101.8, 376 MHz) and Bruker AVANCE III (700, 176 MHz) at 298 K with the stated solvents. The chemical shift was given in ppm (reference substance: tetramethylsilane with $\delta = 0.00$ ppm) and calibrated using $CDCl_3$ and DMSO-d6. Confocal laser scanning microscopy (CLSM) was performed using a Leica DMI6000CSB SP8 inverted confocal laser-scanning microscope (Leica, Wetzlar, Germany) with a 63x/1.4 HC PL APO CS2 oil immersion objective using the manufacture-given LAS X software. Fluorescence spectra of the samples were obtained using a Varian Cary Eclipse fluorescence spectrophotometer using a cell with a 1.0 cm path length. The cytotoxicity of the compounds was analyzed using the cell viability assay Cell Counting Kit 8 (CCK-8) from Sigma-Aldrich Chemie GmbH (Taufkirchen, Germany), according to the manufacturer's instructions. The size of the NGs in aqueous solution was measured using a Zetasizer)Nano ZS(analyzer with an integrated 4 mW He–Ne laser at a wavelength of 633 nm with a backscattering detector angle of 173° (Malvern Instruments Ltd., Worcestershire WR14 1XZ, United Kingdom) at 25 °C and Zeta PALSS for the zeta potential test. The concentration of the samples for the dynamic light scattering (DLS) and zeta potential experiments was 0.05 mg/mL in PBS (pH 7.4) and the samples were measured at 25 °C. Aqueous solutions were filtered via 0.45 μm polytetrafluoroethylene (PTFE) filters and used for DLS measurements. Electrochemical analyses were obtained using an Autolab Potentiostate/Galvanostate model PGSTAT 204 (Eco Chemie, The Netherlands) that was computer-controlled with NOVA 2.1 software. Electrochemical impedance measurements were carried out on a frequency response detector model 1025 interfaced to an EG&G 263 A potentiostate/galvanostate via GPIB on a PC running power suite. EIS spectra were collected at open circuit potential with 10 mV rms AC amplitude at scanned frequencies from 100 kHz to 1 Hz. Three electrode systems were used, including the modified gold electrode, platinum wire, and saturated calomel reference electrode (SCE) as the working, auxiliary, and reference electrodes, respectively. A Metrohm model 713 pH-meter (Herisau, Switzerland) was used for pH measurements and an ultrasound bath with temperature control (50 Hz Soner 203 H; Rocker; Taiwan) was used for sonicating the materials.

4. Experimental

4.1. Synthesis of PEG-triazine-CD (PEG-g-CD)

6-O-Monotosyl-6-deoxy-β-CD (TSO-β-CD) was synthesized using a reported procedure in the literature. For this purpose, β-CD (5.00 g, 4.5 mmol) and p-toluenesulfonic anhydride (2.10 g, 6.47 mmol) were dispersed in 45 mL deionized water. The suspension was stirred for 2 h at room temperature. Then, sodium hydroxide (0.1 mol/L, 25 mL) was added to the reaction mixture. After 10 min, unreacted p-toluenesulfonic anhydride was removed by filtration. The filtrate was neutralized by hydrochloric acid (4 M). 6-OMonotosyl-6-deoxy-β-CD (TSO-β-CD) (2.50 g, 44%) was collected after cooling the solution overnight to 4 °C. The product was dried under vacuum for 72 h at 4 °C.

Afterwards, TSO-β-CD (1.5 g, 1.17 mmol) was dissolved in ethylenediamine (5 mL, 75.87 mmol) under an argon atmosphere. The mixture was stirred at 60 °C for 12 h. Then, the obtained mixture was cooled at room temperature and precipitated in 100 mL ethanol. The product, 6-O-aminoethylamino-6-desoxy-β-CD (β-CD-ene), was collected by filtration and dried at room temperature (77%) (Fig. 1a).

Then, poly (ethylene glycol) 2000 (10 g, 5 mmol) and sodium hydroxide (0.2 g, 5 mmol) were dissolved in water (20 mL). The solution was slowly added to cyanuric chloride (0.92 g, 5 mmol) in 100 mL dichloromethane at 0 °C. The reaction mixture was stirred for 24 h at room temperature. Then, it was refluxed for 6 h, filtered, and the solvent was evaporated. The product was dissolved in 10 mL dichloromethane and precipitated in diethyl ether to obtain 2-(methoxy-polyethylene-2000)− 4,6-dichlorotriazine (PEG-DCT) (41%).

Finally, for the synthesis of PEG-triazine-CD (PEG-g-CD), PEG-DCT (0.51 g, 0.1 mmol) and β-CD-ene (0.57 g, 0.5 mmol) were dispersed in deionized water (10 mL) at room temperature and stirred for 2.5 h. Afterwards, the temperature was increased to 60 °C and the reaction mixture was stirred overnight, then solution was cooled down and dialyzed. The solvent was evaporated and the product was dried (Fig. 1b).

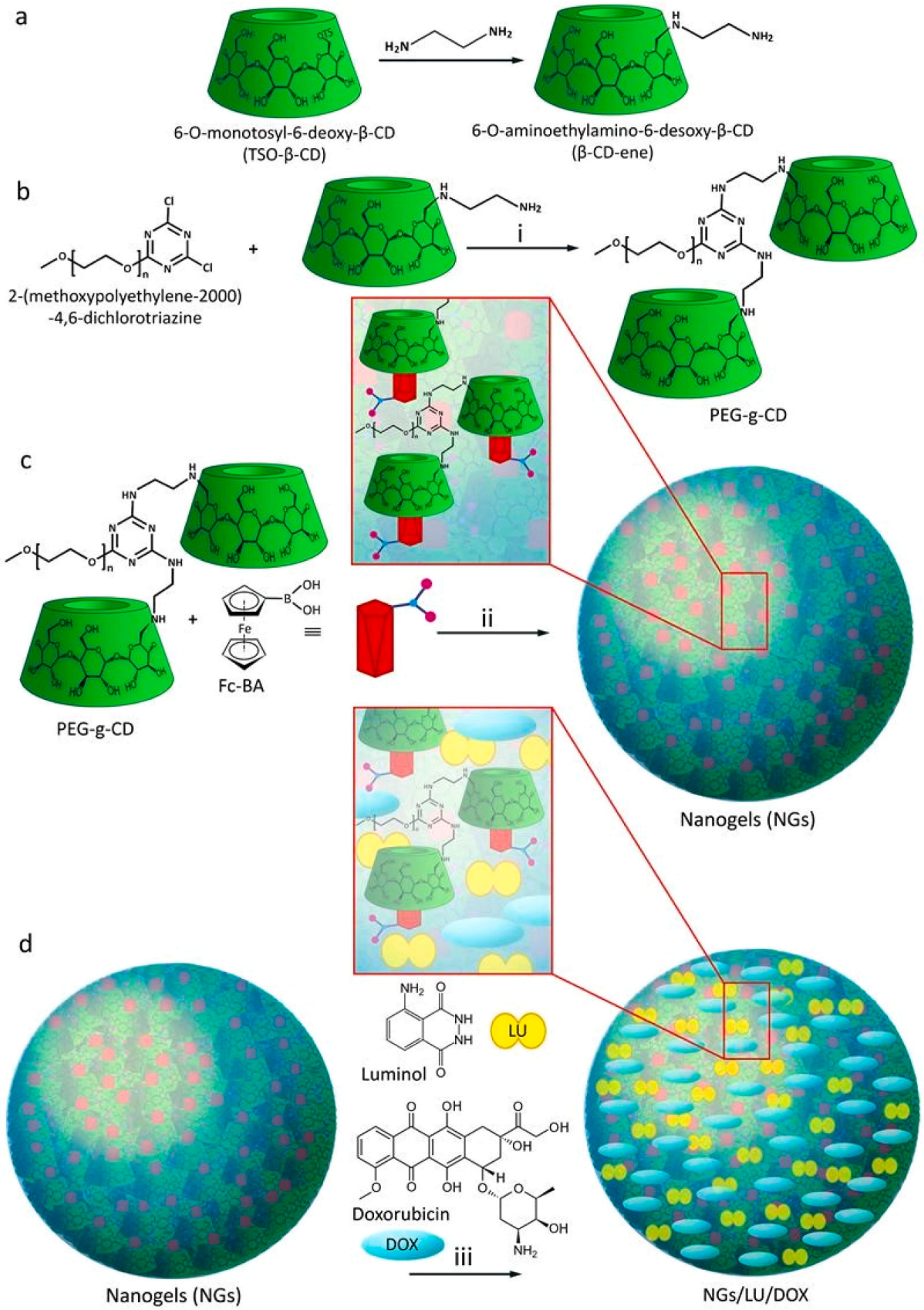

Fig. 1. Schematic representation of the synthesis of (a) 6-O-aminoethylamino-6-desoxy-β-CD. (b) PEGtriazine-CD (PEG-g-CD). (c) Preparation of NGs upon host-guest interactions between PEG-g-CD and FcBA. (d) NG was able to be loaded with DOX and LU to obtain the final theranostic system. (i) PBS (pH 8) at room temperature for 48 h; (ii) water and NaOH for 24 h; (iii) water and NaOH at room temperature for 24 h in the dark.

4.2. Synthesis of nanogels (NGs)

In order to synthesize the NG, FcBA (0.016 g, 0.07 mmol) and PEG-triazine-CD (0.446 g, 0.01 mmol) were dissolved in 50 mL of PBS (pH 8). The obtained mixture was stirred at room temperature for 48 h. Then, the reaction mixture was dialyzed against methanol and deionized water with a 2 kDa MWCO membrane for 24 and 48 h, respectively. The yield of the reaction was almost 100% (Fig. 1**c**).

4.3. Preparation of DOX-Loaded NG (NG/DOX), LU-Loaded NG (NG/LU), and NG/LU/DOX

NG was loaded with DOX using a solvent evaporation method. The NG (0.015 g) was dispersed in buffer at pH 7.4 and DOX (0.005 g, 0.9×10^{-5} mmol) was added to methanol (2 mL). These solutions were mixed and stirred for 24 h. Then, the mixture was centrifuged at 12,000 rpm for 15 min to remove free DOX. Eq. (1) was used to calculate the encapsulation efficiency (EE) of DOX by the NG [53]:

$$EE(\%) = \frac{De}{Dt} \times 100 \quad (1)$$

where De is the amount of the encapsulated drug into the NG and Dt is the total amount of the added drug.

LU (0.025 mol/L, 1 mL) was added to the aqueous solution of NG (5 mL), cooled at room temperature, and stirred for 12 h in darkness. Then, the obtained solution was centrifuged at 12,000 rpm for 10 min to remove free LU. The product was then dried under vacuum at 40 °C and the amount of loaded LU was calculated using the above-mentioned equation.

DOX/LU/NG was prepared as follows: DOX (0.005 g, 0.9×10^{-5} mmol) and LU in aqueous solutions of NaOH (0.025 mol/L, 1 mL) were incubated with an aqueous solution of NG (5 mL) in darkness for 24 h. Then, the solution was centrifuged at 12,000 rpm for 10 min to remove free DOX and LU (Fig. 1d). The amount of loaded DOX was calculated using the above-mentioned equation.

4.4. Release of DOX from NG

NG/DOX (0.02 g) was dispersed in 3 mL of buffer (pH 7.4) and placed in a dialysis bag.

(MW 2000) with a controlled temperature at 37 °C. Then, the dialysis bag was placed in 50 mL PBS (pH 7.4). At regular time intervals, 2 mL of outer solution was removed and replaced with fresh PBS to preserve the sink condition and the absorbance of the released drug was recorded using UV-Vis spectroscopy at 480 nm. The amount of drug released was obtained through a calibration curve. The evaluation of drug release was investigated in two conditions (in the absence and presence of H_2O_2). The latter was carried out by adding 0.2 μL of H_2O_2 (0.88 M) to the PBS (pH 7.4, 50 mL). According to Eq. (2), the effective release of DOX from the NG was calculated as follows [54]:

$$\text{Drug Release Efficiency}\left(\%\right) = \frac{\text{Dr}}{\text{De}} \times 100 \quad (2)$$

where Dr is the amount of drug released from the NG and De is the amount of drug encapsulated into the NG.

4.5. Fluorescence silencing study

Samples, including NG/LU and NG/LU/DOX, were prepared in 0.1% PBS buffer (pH 8) and mixed with different concentrations of H_2O_2 diluted with 0.1% PBS buffer (pH 8). The fluorescence emission of different samples was measured at 37 °C using a Cary Eclipse fluorescence spectrophotometer (Varian, Australia). Samples were excited at wavelengths of 350 nm and 400–600 nm. The slit width was 2.5 nm. The quantitative calculation of the.

LOD for the NGs was performed using the calibration curve with the following equation.

[55]:

$$\text{LOD} = \frac{(3 \times \text{S})}{\text{B1}} \quad (3)$$

where B1 is the slope of the calibration curve line and S is the standard deviation of the minimum concentration.

4.6. Cyclic voltammogram study

Cyclic voltammetry (CV) with voltage range of − 0.2–0.7 V (SCE) was performed at various potential scan rates of 100 mVs^{-1}. To obtain the cyclic voltammograms, PBS solution containing tetra-n-butylammonium tetrafluoroborate (0.1 M) was used as the supporting electrolyte and a three-electrode system consisting of a glassy carbon working electrode, a Pt counter electrode, and an Ag/AgCl reference electrode were utilized in a singlecomponent electrochemical cell. They were immersed in 1 M HCl or 1 M H_2SO_4 electrolyte solution. All experiments were performed at room temperature. In this work, we used tetraethyl ammonium tetrafluoroborate solution (TEATFB, 0.1 M) containing 0.1 M potassium chloride as the supporting electrolyte. For this purpose, 0.1 g of tetraethyl ammonium tetrafluoroborate was dissolved in 5 mL of DMSO. Then, the TEATFB solution was added to 5 mL aqueous solution containing potassium chloride (0.1 M) to achieve a 1:1 solution of DMSO/water. Then, a solution of 10 mM polymer (0.1 mL) was added to the FcBA solution with excess electrolyte and the cyclic voltammogram (CV) peak was recorded several times. To avoid the dilution effect in all electrochemical experiments, polymer stock solutions containing FcBA (1 mM) were added to the solution of FcBA (1 mM).

4.7. Cytotoxicity study

The cytotoxicity of the NGs against MCF-7 cells was studied using the CCK-8 assay. Cells were seeded onto a 96-well plate at a density of 1×10^4 cells per well in 100 μL of RPMI 1640 medium containing FBS (10%) and penicillin-streptomycin (1%) and incubated for 24 h at 37 °C in a CO_2 (5%) atmosphere. Afterwards, the stale medium was removed and replenished with 90 μL of fresh medium. Then, 10 μL of NG sample at different concentrations in DPBS was added to each sample well. Then, the plate was incubated for 24 h at 37 °C in a CO_2 (5%) atmosphere. A 10 μL aliquot of CCK-8 solution was added to each well and the plate was incubated for 3 h. Ultimately, the percentage of cell viability was calculated after recording the absorbance of the samples at 450 nm using a microplate reader (Infinite 200 Pro plate reader; Tecan Group Ltd., Männedorf, Switzerland) using the following equation [56]:

$$\text{Cell viability}\left(\%\right) = \frac{(\text{As} - \text{Ab})}{(\text{Ac} - \text{Ab})} * 100 \quad (4)$$

where As, Ab and Ac are the absorbances of the sample, blank, and control, respectively.

The reference wavelength was 620 nm.

4.8. Confocal study

Uptake of the NG by MCF-7 cells was evaluated by confocal laser scanning microscopy (CLSM). MCF-7 cells were seeded onto a 8-well plate at a density of 1×10^4 cells per well in 300 μL medium and cultured for 24 h at 37 °C in a 5% CO_2 atmosphere. Then, 10 μL of NG solution with a concentration of 3 mg/mL was added to the medium and cultured for another 6 h at 37 °C in a 5% CO_2 atmosphere. Afterwards, the samples were washed once with the cell culture medium and twice with PBS (pH 7.4), followed by fixing with paraformaldehyde (4%) at room temperature for 15 min. Then, the samples were washed 3 times

with cold PBS and incubated in darkness for another 15 min in a solution of DAPI (1:4000). Finally, the samples were washed twice with PBS and imaged by a confocal microscope connected to VivaScan computer software (Version 11.0.1140).

5. Results and discussion

5.1. NG synthesis and characterization

Theranostics combining the treatment and diagnosis of cancer cells have attracted a great deal of attention in cancer therapy. Nanoparticles, due to their excellent physicochemical and biological properties, are useful platforms to construct theranostic systems [69]. Owing to their high stability and biocompatibility, supramolecular PNGs are excellent candidates for this purpose, among the different types of nanoparticles [15,70]. NGs are often composed of bio- or synthetic polymers that are physically or chemically crosslinked to make a network [71–74]. By binding a "host" reversibly to a "guest" molecule, hostguest interactions can form highly complex and ordered structures as well as polymeric networks [75–77]. Fc, as the most common electroactive guest, inserts in CD cavities and forms host-guest complexes [78]. Accordingly, in the present study, a series of NGs was prepared using host-guest interactions between the PEG-g-CD molecule as the host and FcBA as the guest molecule, which were loaded with DOX and LU for the simultaneous detection and treatment of cancer cells. FcBA plays several roles, including physical crosslinking by host-guest interactions, boronate ester formation, as well as interaction with cancer cells via cis-diol configuration of overexpressed polysaccharides [79].

Successful NG synthesis and drug loading were confirmed through FTIR, UV-Vis, and ^{1}HNMR spectroscopy. As shown in the IR spectrum of FcBA (Fig. 2Aa), the absorption bands at 1500 and 1045 cm^{-1} were attributed to the stretching vibrations of the ferrocenyl ring. Furthermore, bands at 1345 and 1375 cm^{-1} were attributed to the B-O vibration and bands at 3360 and 3650 cm^{-1} demonstrated the presence of hydroxyl groups. In IR spectrum of PEG-g-CD, the absorption bands in the regions of 1458 cm^{-1} and 1271 cm^{-1} were related to the stretching vibrations of C═N and C-N in triazine, respectively (Fig. 2 Ab). In the IR spectrum of the NGs (Fig. 2 Ac), the presence of absorption bands of FcBA and PEG-gCD with small displacements represented their supramolecular assemblies in the form of nanoparticles. There were absorption bands at 3200, 3600, and 1400–1750 cm^{-1} for NG/DOX (Fig. 2 Ad), corresponding to the OH, N-H, C═O, and C═C stretching vibrations, respectively.

The UV-Vis spectra of the NG, NG/LU, NG/LU/DOX, and LU are shown in Fig. 2B. The UV-Vis spectrum of LU showed two absorption peaks at 293 and 340 nm [57]. Nevertheless, two red-shifted absorption peaks were obtained for NG/LU/DOX compared with LU, and the intensity of the absorption peak was significantly increased, indicating the successful loading of LU into NG/LU/DOX. Additionally, in the UV-Vis spectrum of NG/LU/DOX, a new absorption peak at 500 nm corresponded to DOX [58]. This peak was another indication of the attachment of DOX on the NG.

NMR spectroscopy was used to further evaluate the structure of prepared nanoparticles. Protons related to β-cyclodextrin in *β*-CD-OTS was appeared between 3.5 and 5.8 ppm (aliphatic protons H-1 (4.9 ppm), H-3, H-5 (3.5 ppm), and H-6 (3.6 ppm) and hydroxyl groups (OH-2, OH-3 (5.7 ppm), and OH-6 (4.5 ppm)). Also ^{1}H NMR spectrum of the *β*-CD-OTS indicated two peaks between 7 and 8 ppm which related to -OTS groups. The decrease in peak intensity in 7–8 ppm of *β*-CD-ene indicates the binding of ethylenediamine to cyclodextrin of *β*-CD-OTS. The protons of the methoxy polyethylene glycol group was appeared in the region of 2.37 ppm. The methylene groups of polyethylene glycol

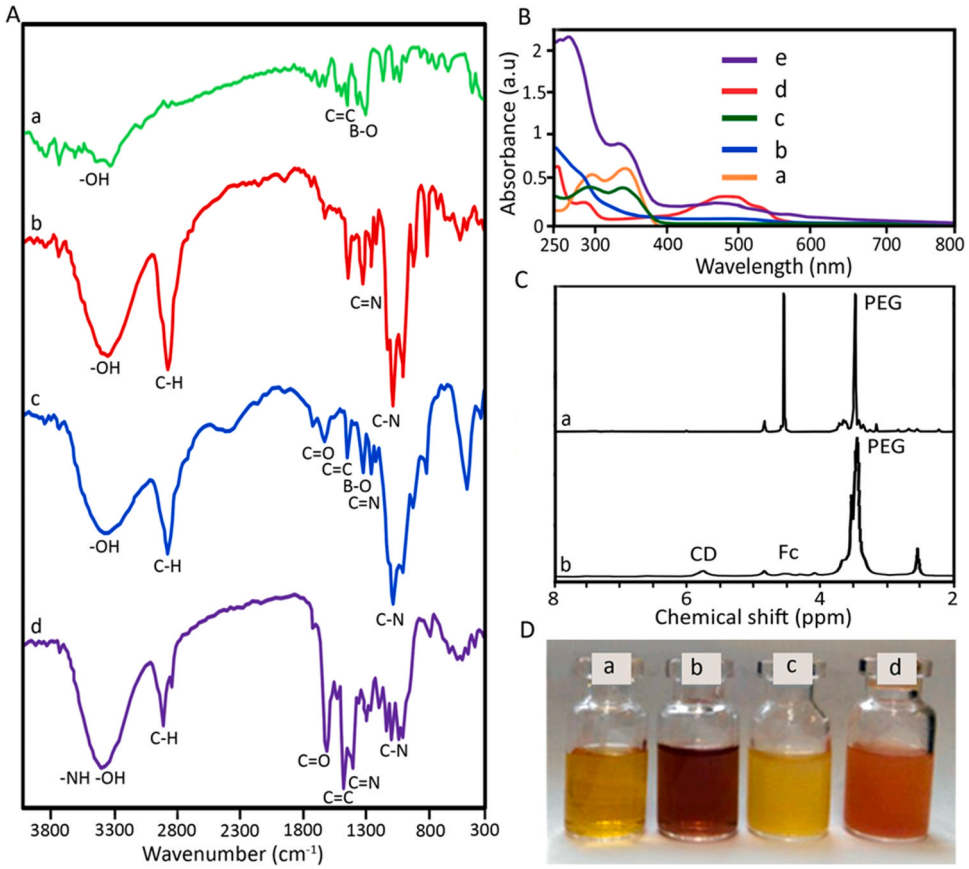

Fig. 2. (A) The IR spectra of (a) FcBA, (b) PEG−g−CD, (c) NG, and (d) NG/DOX. (B) UV−Vis spectra of (a) LU, (b) NG, (c) NG/LU, (d) DOX and (e) NG/LU/DOX. (C) 1 H NMR spectrum of (a) PEG-triazine-β-CD and (b) NG. (D) Images of (a) NG, (b) NG/DOX, (c) NG/LU, and (d) NG/LU/DOX.

have appeared in the region of 3.6–3.7 ppm that showed chemical shift in the final product. Due to the large number of protons related to PEG segments compared to the β-CD, β-CD's peaks did not appear well in PEG-g-CD spectrum. Generally, the hydrogens of hydroxyl groups of BA appear in the range of 8–9.7 ppm [59], but they disappear upon esterification. Disappearing peaks of these protons in the spectra of the NGs indicated conjugation of Fc to CD by boronate ester bonds. Additionally, signals at 4.2– 4.8 and 3.7 ppm corresponded to Fc and PEG segments, respectfully. Protons of the CD segment appeared at 5.7–5.9 ppm. In the presence of the Fc ligand, the CD protons were shifted to the lower field, which was the result of host-guest interactions between Fc and β-CD (Fig. 2 C). In addition, digital images of NG, NG/DOX, NG/LU, and NG/LU/DOX are shown in Fig. 2D, displaying the color change in the NG after DOX and LU loading.

5.2. Fluorescence silencing

The results showed that incubation of NG/LU and NG/LU/DOX with different levels of H_2O_2, as the main ROS component in cancerous tissues and blood, led to a dramatic quenching of the fluorescence emission of LU. As expected, by increasing the H_2O_2 concentration, the fluorescence of NG/LU significantly decreased which confirmed the oxidation of LU by H_2O_2. Changes in the fluorescence intensity of NG/LU/DOX upon increasing H_2O_2 concentration were also investigated. The observed results were similar to those of NG/LU (Fig. 3 A(a,b)). As shown in Fig. 3B, H_2O_2 oxidized Fc and LU to ferrocenium and 3-aminofetalate, respectively. The produced ferrocenium ion, as an electron acceptor, quenched the excited state of LU, as an electron donor (3-aminophtalat intermediate), through the electron transfer mechanism (PET) [60–64].

To describe the quenching mechanism of LU, the fluorescence data were analyzed using the Stern-Volmer Equation [65,66]:

$$\frac{F_0}{F} = 1 + K_{SV}[Q] \quad (6)$$

where F and F0 refer to the intensity of the fluorescence detector peaks in the presence and absence of the quenching agent, respectively; Ksv is the Stern-Volmer constant; and [Q] is the quenching concentration (Fig. 4B). The quenching constant of NG/LU was larger than that of NG/LU/ DOX, indicating the great potential of the NG loaded with LU for the detection of cancer cells using the fluorescence signal.

5.3. DLS, SEM and TEM analysis

The hydrodynamic dimensions of the NG and NG/DOX were investigated by DLS measurements (Fig. 4 C). The results indicated an increase in the hydrodynamic diameter of the NG after loading with DOX from 280 to 460 nm confirming successful drug loading. This result indicated that DOX molecules interfered with the host-guest interactions between FcBA and CDs and enlarged the system with dissociation of some of these interactions. This was consistent with similar systems in the literature, where co-loading of laparib and doxorubicin in disulfide bond-crosslinked polypeptide NGs efficiently increased their size [80]. The DOX encapsulation efficiency was calculated to be 45.65%. The

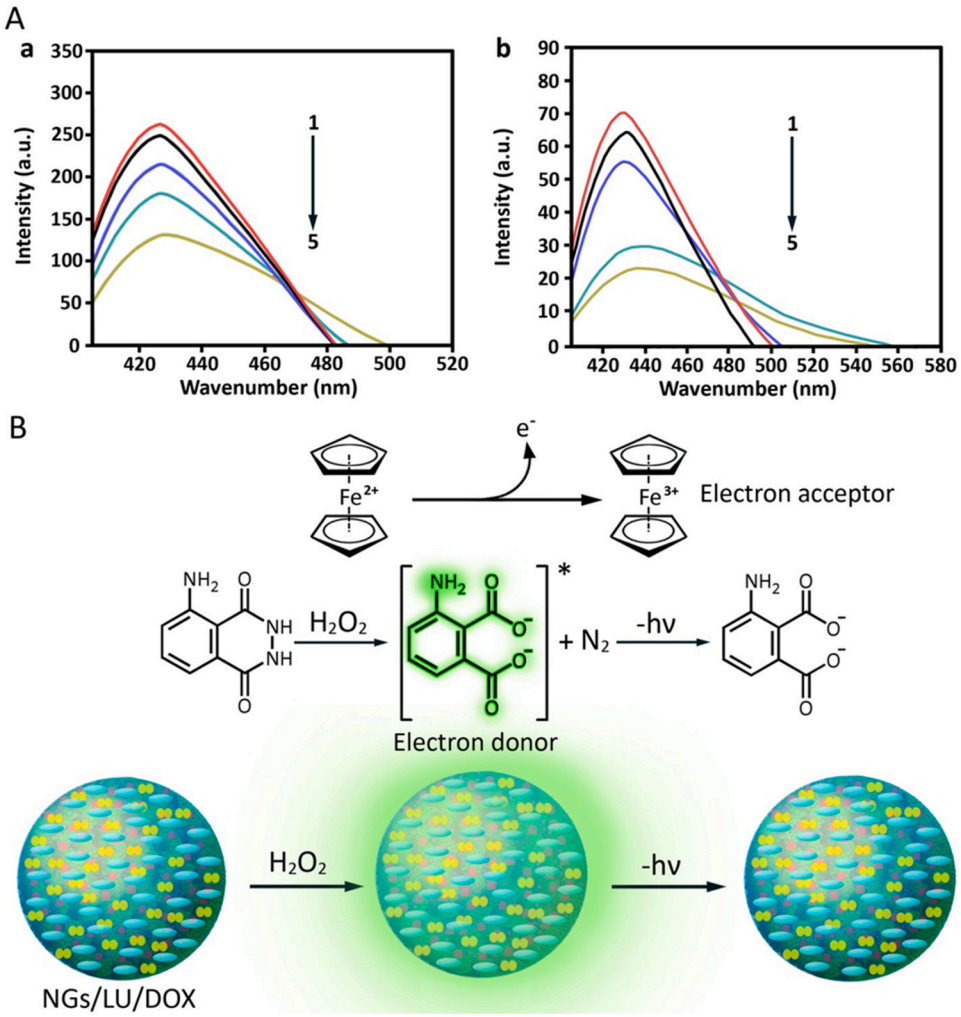

Fig. 3. (A) Fluorescence quenching at 428 nm for (a) NG/LU and (b) NG/LU/DOX by adding different concentrations of H_2O_2 at 37 °C and pH 8. The concentration of H_2O_2 was increased as follows: (1) 5.8×10^{-6}, (2) 16×10^{-6}, (3) 32×10^{-6}, (4) 45×10^{-6}, and (5) 64×10^{-6} M. The fluorescence intensity of NG/LU and NG/LU/DOX decreased upon increasing H_2O_2 concentration. The results indicated the oxidation of LU by H_2O_2. (B) Schematic representation of the mechanism of fluorescence quenching of LU by ferrocene.

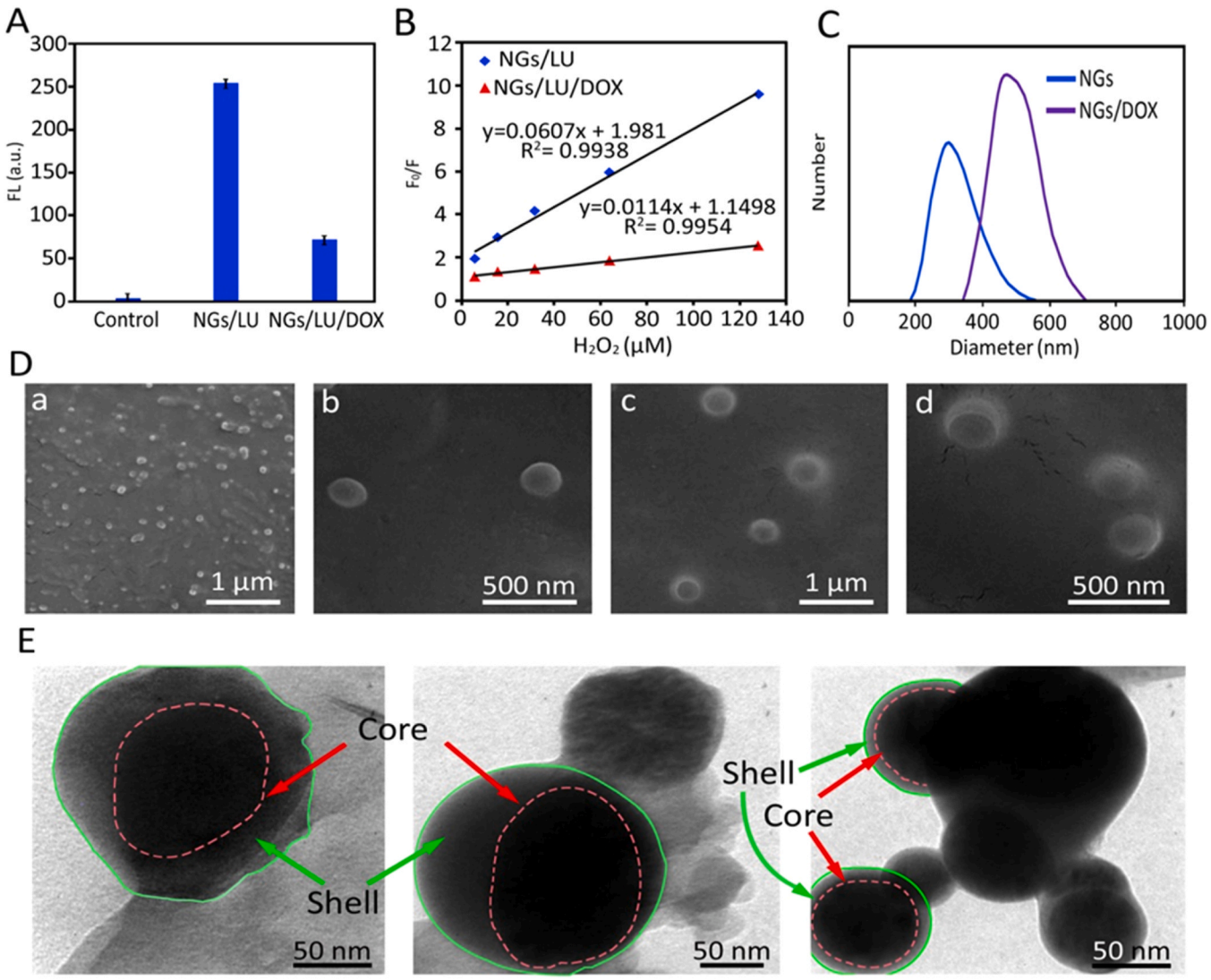

Fig. 4. (A) Comparison of the fluorescence intensity of buffer, NG/LU, and NG/LU/DOX. Buffer (as control) did not show significant fluorescence intensity compared to NG/LU and NG/LU/DOX. (B) SternVolmer plots for LU quenching at 25 °C with different concentrations of H_2O_2, demonstrating the higher quenching constant of NG/LU compared with that of NG/LU/ DOX. (C) SEM images of NG (a,b), and NG/DOX (c,d) at magnitudes of 1 μm and 500 nm (D) TEM images of the NG showing the core-shell structure. While the darker part is estimated to be mainly composed of ferrocene segments, the brighter shell consists of polymer.

surface charge of the NG and NG/DOX was investigated using zeta potential analysis. As shown in Table S1, the surface charge of the NG was − 15 ± 3 mV. This value was − 11 ± 2 mV for NG/DOX, demonstrating loading of DOX molecules by the NG and decreasing the negative charge of the NG. The surface charge of NG/LU was − 23 ± 3 mV. Based on these results, the increased concentration of oxidized LU led to an increase in the negative surface charge of the NG. In the case of NG/LU/DOX, DOX loading led to a reduction in the negative surface charge compared to NG/LU. DOX loading, because of the amino functional groups of this drug, decreased the negative charge of the nanogel from − 15 mV to − 11 mV. This has been observed in similar studies, where DOX loading dramatically changed the zeta (ζ) potential of the original NG[81]. LU loading, due to the oxidation of some of the LU molecules and formation of carboxylic groups, increased the negative charge of the NG from − 15 mV to − 23 mV. The negative surface charge of the NG was related to the presence of free hydroxyl groups on the outer surface of CDs.

The morphology of the NG and NG/DOX was evaluated using FE-SEM. As shown in Fig. 4 D, the NG demonstrated a core-shell spherical structure with a size of 100–200 nm. Accumulation of FcBA in the center of the assembly led to a dark core and polymer in the outer part created a more transparent shell. According to Fig. 4D (c,d), NG loaded with DOX displayed larger dimensions (250–350 nm) compared with the unloaded NG. The TEM images also showed spherical nanoparticles with an average size of approximately 80 nm and with a core-shell structure (Fig. 4E). The dark and bright core and shell consisted of ferrocene and polymer, respectively. According to the TEM images, the size of DOX-loaded NG was ~267 nm, which was larger than the unloaded NG (~120 nm). This result confirmed partial dissociation of the NG upon loading of DOX molecules inside CD cavities. The difference between the sizes of the NG in solution and dry corresponded to their supramolecular and dynamic structures.

5.4. Cyclic Voltammetry (CV) study

To confirm the formation of host-guest interactions, cyclic voltammetry (CV) was performed and alterations in anodic and cathodic flows (the cause of interaction) were evaluated. Cyclic voltammetry (CV) confirmed the inclusion of FcBA as a guest in the CD cavity as a host molecule. The results demonstrating a decrease in peak flow of CV of the guest sample (FcBA) at each step of host (polymer) addition. When the electrode level was corrected, peak flow increased substantially,

indicating an improvement in electron transfer by the NG. As shown in Fig. 5Aa, the electrochemical behavior of the Fc/β-CD complex was similar to that of Fc, but the peak potentials were displaced to more positive values, which was dependent on the concentration of β-CD. Decreases in both anodic and cathodic peaks were observed with increased concentration of β-CD, which represented the process of reversible electron transfer. Oxidation and reduction of the NG were more difficult than those of its ligands, which was due to the blockage of the β-CD ring that led to the displacement of peak potentials [67].

5.5. Release study

The release of a therapeutic agent from the NG was evaluated. The loaded drug was significantly sensitive to a low concentration of H_2O_2 (0.05 mM) and demonstrated higher release in the presence of H_2O_2 at 37 °C. This result indicated the redox stimuli-responsivity of the NG. It was found that more than 90% DOX was released in three hours upon the addition of 0.05 mM H_2O_2 (Fig. 5 Ab). The concentration of reactive oxygen species (ROS), including H_2O_2, superoxide anions, and hydroxyl radicals, in tumor microenvironments is higher than that in healthy systems [82]. For example, the concentration of H_2O_2, as a main ROS component, is approximately 100 mM in malignant tumor cells, whereas this value in normal cells is less than 20 nM [83]. The higher concentration of ROS in cancerous tissues compared with that in healthy counterparts has been used as a stimuli factor to trigger the release of therapeutic and sensing agents for the efficient treatment and detection of cancer cells. The sensitivity of release of the loaded drug to a low concentration of H_2O_2 (0.05 mM) at 37 °C demonstrated the redox stimuli-responsivity of the NG. The oxidation of iron by hydrogen peroxide increased the hydrophilicity of Fc and decreased its affinity for the CD cavity. Therefore, the NG was dissociated by excluding Fc from CD and the cargo was quickly released in a controlled manner. In other studies, Fc-based nanoparticles displayed redox-responsive behavior and the release of DOX from these nanoparticles was efficiently increased in the presence of H_2O_2 (0.4 M) [84]. However, premature release was detected at physiological pH (~60% in 1 h), which may have been due to the nature of the supramolecule or physical adsorption of the drug on the NG. This can adversely affect the therapeutic efficiency of the system but can be improved by partial covalent crosslinking.

5.6. Cytotoxicity and CLSM analysis

To evaluate the biocompatibility of the NG, the in vitro cytotoxicity of the prepared NGs was investigated using a standard counting CCK-8 assay on MCF-7 cells. As shown in.

Fig. 5B, NG at concentrations up to 1000 μg/mL displayed no significant cytotoxicity against MCF-7 cells, indicating the high biocompatibility of the NG and demonstrating its suitability for in vivo applications.

The intracellular distribution of NG and NG/LU/ DOX was investigated by incubating the NG with MCF-7 cells, followed by imaging with a CL-SEM microscope. The images demonstrated the uptake of NG by cells and their localization in the cytoplasm near the cell nucleus (Fig. 5C). The observed green signals in the nucleus of the cells were probably due to the entrance of small pieces of polymer or released FITC [68]. In order to investigate the ability of the NG to transport drugs into the cells, the release of DOX inside the cells was evaluated via CLSM microscopy. The results indicated the transport of DOX by the NG across the cell membranes and localization of this agent around the nucleus using Hoechst staining (Fig. 5C). Overall, CLSM analysis demonstrated uptake of NG by cells and its localization in the cytoplasm near the cell nucleus.

5.7. Conclusions

In this work, a new supramolecular redox-responsive system was developed through hostguest interactions between PEG-g-CD and FcBA and co-loaded with DOX and LU simultaneously. The obtained system demonstrated redox responsiveness. Owing to its high loading capacity, biocompatibility, and fast response to H_2O_2, the produced supramolecular redox-responsive system can be used as a smart theranostic agent for future biomedical applications.

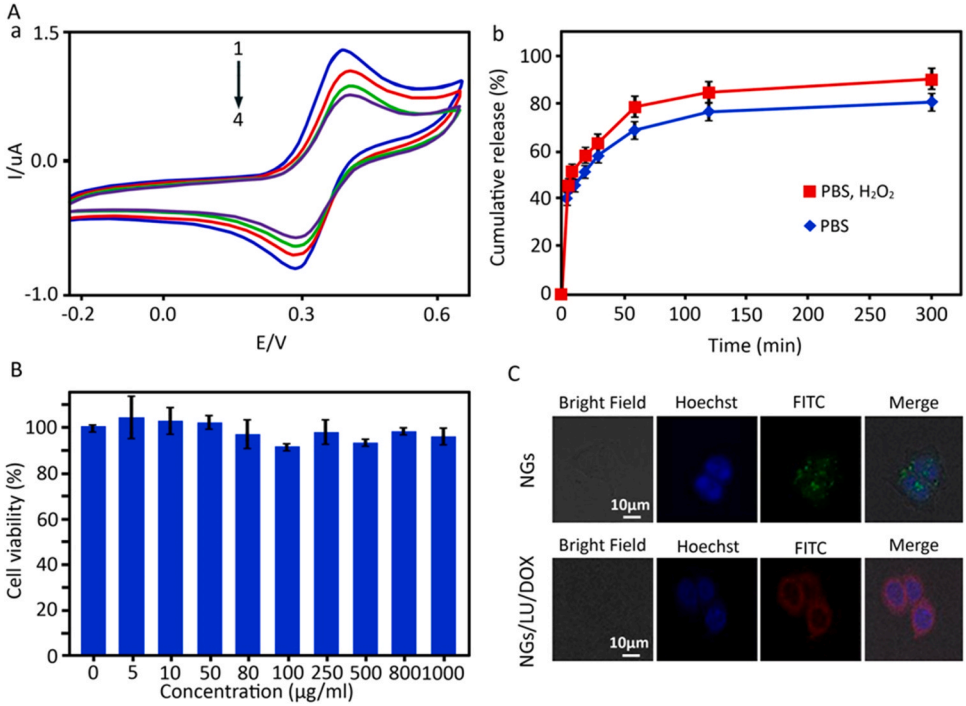

Fig. 5. (A) (a) Cyclic voltammogram of 0.1 mM FcBA in the absence of β-CD polymer (1), in the presence of 0.2 mL of β-CD polymer (10 mM) (2), 0.4 mL of NG (10 mM) (3), 0.6 mL NG (10 mM), and (4) in DMSO/H_2O solvents containing 0.1 M TEATFB. (b) Release profile of loaded DOX from NG in PBS at pH 7.4 with and without incubation with H_2O_2 (0.05 mM). (B) Cytotoxicity of NG against MCF-7 cells following 24 h incubation. All data are presented as the average ± SD (N = 4). (C) Confocal laser scanning microscopy (CLSM) images of NG loaded with FITC (upper row) and NG/ LU/ DOX (lower row), incubated with MCF-7 cells at 37 °C for 6 h.

Funding

This research was funded by Iran National Science Foundation, Tehran, Iran (Postal Code: 1439634665). (INSF Grant ID NO. G4001281).

CRediT authorship contribution statement

Mohsen Adeli, Abdollah Yari, Zainab Ahmadian: Conceptualization. **Mohsen Adeli**: Methodology, Investigation, Visualization, Supervision, Project administration, Funding acquisition. **Siamak Beyranvand**: Software. **Azim Shams, Zeinab Souri, Abbas Faghani**: Validation. **Mohsen Adeli, Zainab Ahmadian**: Formal analysis, Resources. **Khadijeh Soleimani**: Data curation. **Zainab Ahmadian**: Writing – original draft preparation. **Zainab Ahmadian, Khadijeh Soleimani**: Writing – review & editing. All authors have read and agreed to the published version of the manuscript.

Declaration of Competing Interest

The authors declare that they have no known competing financial interests or personal relationships that could have appeared to influence the work reported in this paper.

Acknowledgments

The authors would like to thank the Iran National Science Foundation (INSF) for financial support (grant number 4001281).

Appendix A. Supporting information

Supplementary data associated with this article can be found in the online version at doi:10.1016/j.biopha.2023.115402.

References

1 H. Mollasalehi, E. Shajari, A colorimetric nano-biosensor for simultaneous detection of prevalent cancers using unamplified cell-free ribonucleic acid biomarkers, Bioorg. Chem. 107 (2021), 104605.
2 E. Mohammadifar, A.N. Kharat, M. Adeli, Polyamidoamine and polyglycerol; their linear, dendritic and linear–dendritic architectures as anticancer drug delivery systems, J. Mater. Chem. B 3 (2015) 3896–3921.
3 T. Alon-Maimon, O. Mandelboim, G. Bachrach, Fusobacterium nucleatum and cancer, 2000, Periodontology 89 (2022) 166–180.
4 S. Sargazi, E. Simge, A. Mobashar, S.S. Gelen, A. Rahdar, N. Ebrahimi, S. M. Hosseinikhah, M. Bilal, G.Z. Kyzas, Aptamer-conjugated carbon-based nanomaterials for cancer and bacteria theranostics: A review, Chem. -Biol. Interact. 361 (2022), 109964.
5 N.V. Rao, H. Ko, J. Lee, J.H. Park, Recent progress and advances in stimuliresponsive polymers for cancer therapy, Front. Bioeng. Biotechnol. 110 (2018) 110.
6 R. Kumar, A. Kulkarni, D.K. Nagesha, S. Sridhar, In vitro evaluation of theranostic polymeric micelles for imaging and drug delivery in cancer, Theranostics 2 (2012) 714.
7 M.S. Muthu, S.-S. Feng, Theranostic liposomes for cancer diagnosis and treatment: Current development and pre-clinical success, Expert Opin. Drug Deliv. 10 (2013) 151–155.
8 M. Wang, Y. Zhang, M. Ng, A. Skripka, T. Cheng, X. Li, K.K. Bhakoo, A.Y. Chang, F. Rosei, F. Vetrone, One-pot synthesis of theranostic nanocapsules with lanthanide doped nanoparticles, Chem. Sci. 11 (2020) 6653–6661.
9 M. Ghezzi, S. Pescina, C. Padula, P. Santi, E. Del Favero, L. Cantù, S. Nicoli, Polymeric micelles in drug delivery: An insight of the techniques for their characterization and assessment in biorelevant conditions, J. Control Release 332 (2021) 312–336.
10 J.K. Alwattar, A.T. Mneimneh, K.K. Abla, M.M. Mehanna, A.N. Allam, Smart stimuliresponsive liposomal nanohybrid systems: A critical review of theranostic behavior in cancer, Pharmaceutics 13 (2021) 355.
11 Y.-Q. Liu, L.-Y. Qin, H.-J. Li, Y.-X. Wang, R. Zhang, J.-M. Shi, J.-H. Wu, G.X. Dong, P. Zhou, Application of lanthanide-doped upconversion nanoparticles for cancer treatment: A review, Nanomedicine 16 (2021) 2207–2242.
12 S. Sattari, M. Adeli, S. Beyranvand, M. Nemati, Functionalized graphene platforms for anticancer drug delivery, Int. J. Nanomed. 16 (2021) 5955.
13 W. Zhou, G. Yang, X. Ni, S. Diao, C. Xie, Q. Fan, Recent advances in crosslinked nanogel for multimodal imaging and cancer therapy, Polymers 12 (2020) 1902.
14 W. Li, W. Xu, S. Zhang, J. Li, J. Zhou, D. Tian, J. Cheng, H. Li, Supramolecular biopharmaceutical carriers based on host–guest interactions, J. Agric. Food Chem. 70 (2022) 12746–12759.
15 B. Sierra-Martin, A. Fernandez-Barbero, Multifunctional hybrid nanogels for theranostic applications, Soft Matter 11 (2015) 8205–8216.
16 E. Miceli, B. Kuropka, C. Rosenauer, E.R. Osorio Blanco, L.E. Theune, M. Kar, C. Weise, S. Morsbach, C. Freund, M. Calderón, Understanding the elusive protein corona of thermoresponsive nanogels, Nanomedicine 13 (2018) 2657–2668.
17 K. Obst, G. Yealland, B. Balzus, E. Miceli, M. Dimde, C. Weise, M. Eravci, R. Bodmeier, R. Haag, M. Calderón, Protein corona formation on colloidal polymeric nanoparticles and polymeric nanogels: Impact on cellular uptake, toxicity, immunogenicity, and drug release properties, Biomacromolecules 18 (2017) 1762–1771.
18 M. Molina, M. Asadian-Birjand, J. Balach, J. Bergueiro, E. Miceli, M. Calderón, Stimuli-responsive nanogel composites and their application in nanomedicine, Chem. Soc. Rev. 44 (2015) 6161–6186.
19 M. Asadian-Birjand, A. Sousa-Herves, D. Steinhilber, J.C. Cuggino, M. Calderon, Functional nanogels for biomedical applications, Curr. Med. Chem. 19 (2012) 5029–5043.
20 Z. Shatsberg, X. Zhang, P. Ofek, S. Malhotra, A. Krivitsky, A. Scomparin, G. Tiram, M. Calderón, R. Haag, R. Satchi-Fainaro, Functionalized nanogels carrying an anticancer microRNA for glioblastoma therapy, J. Control. Release 239 (2016) 159–168.
21 F. Rancan, M. Asadian-Birjand, S. Dogan, C. Graf, L. Cuellar, S. Lommatzsch, U. Blume-Peytavi, M. Calderón, A. Vogt, Effects of thermoresponsivity and softness on skin penetration and cellular uptake of polyglycerol-based nanogels, J. Control. Release 228 (2016) 159–169.
22 F.B. Ilhami, Y.-T. Yang, A.-W. Lee, Y.-H. Chiao, J.-K. Chen, D.-J. Lee, J.-Y. Lai, C.-C. Cheng, Hydrogen Bond Strength-Mediated Self-Assembly of Supramolecular Nanogels for Selective and Effective Cancer Treatment, Biomacromolecules 22 (2021) 4446–4457.
23 A. Duro-Castano, A. Sousa-Herves, A. Armiñán, D. Charbonnier, J.J. Arroyo-Crespo, S. Wedepohl, M. Calderón, M.J. Vicent, Polyglutamic acid-based crosslinked doxorubicin nanogels as an anti-metastatic treatment for triple negative breast cancer, J. Control. Release 332 (2021) 10–20.
24 M. Zhu, D. Lu, S. Wu, Q. Lian, W. Wang, A.H. Milani, Z. Cui, N.T. Nguyen, M. Chen, L.A. Lyon, Responsive nanogel probe for ratiometric fluorescent sensing of pH and strain in hydrogels, ACS Macro Lett. 6 (2017) 1245–1250.
25 A.E. Ekkelenkamp, M.R. Elzes, J.F. Engbersen, J.M. Paulusse, Responsive crosslinked polymer nanogels for imaging and therapeutics delivery, J. Mater. Chem. B 6 (2018) 210–235.
26 H. Ye, Y. Zhou, X. Liu, Y. Chen, S. Duan, R. Zhu, Y. Liu, L. Yin, Recent advances on reactive oxygen species-responsive delivery and diagnosis system, Biomacromolecules 20 (2019) 2441–2463.
27 K. Harini, P. Pallavi, P. Gowtham, K. Girigoswami, A. Girigoswami, Smart PolymerBased Reduction Responsive Therapeutic Delivery to Cancer Cells. Curr, Pharmacol. Rep. 8 (2022) 205–211.
28 M. Calderón, M.A. Quadir, M. Strumia, R. Haag, Functional dendritic polymer architectures as stimuli-responsive nanocarriers, Biochimie 92 (2010) 1242–1251.
29 J.C. Cuggino, M.C. Strumia, P. Welker, K. Licha, D. Steinhilber, R.-C. Mutihac, M. Calderón, Thermosensitive nanogels based on dendritic polyglycerol and Nisopropylacrylamide for biomedical applications, Soft Matter 7 (2011) 11259–11266.
30 M. Giulbudagian, M. Asadian-Birjand, D. Steinhilber, K. Achazi, M. Molina, M. Calderón, Fabrication of thermoresponsive nanogels by thermo-nanoprecipitation and in situ encapsulation of bioactives, Polym. Chem. 5 (2014) 6909–6913.
31 C. Gerecke, A. Edlich, M. Giulbudagian, F. Schumacher, N. Zhang, A. Said, G. Yealland, S.B. Lohan, F. Neumann, M.C. Meinke, Biocompatibility and characterization of polyglycerol-based thermoresponsive nanogels designed as novel drug-delivery systems and their intracellular localization in keratinocytes, Nanotoxicology 11 (2017) 267–277.
32 P. Sharma, A. Poonia, M. Jangra, Application of Stimuli-Responsive Polymers in Cancer Therapy. In Handbook of Oxidative Stress in Cancer: Therapeutic Aspects, Springer,, Singapore, 2022, pp. 1–15.
33 J.C. Cuggino, M. Molina, S. Wedepohl, C.I.A. Igarzabal, M. Calderón, L.M. Gugliotta, Responsive nanogels for application as smart carriers in endocytic pHtriggered drug delivery systems, Eur. Polym. J. 78 (2016) 14–24.
34 M. Asadian-Birjand, J. Bergueiro, F. Rancan, J.C. Cuggino, R.-C. Mutihac, K. Achazi, J. Dernedde, U. Blume-Peytayi, A. Vogt, M. Calderón, Engineering thermoresponsive polyether-based nanogels for temperature dependent skin penetration, Polym. Chem. 6 (2015) 5827–5831.
35 L.E. Theune, J. Buchmann, S. Wedepohl, M. Molina, J. Laufer, M. Calderón, NIRand thermo-responsive semi-interpenetrated polypyrrole nanogels for imaging guided combinational photothermal and chemotherapy, J. Control. Release 311 (2019) 147–161.
36 P. Kumar, B. Liu, G. Behl, A comprehensive outlook of synthetic strategies and applications of redox-responsive nanogels in drug delivery, Macromol. Biosci. 19 (2019) 1900071.
37 H.F. Abed, W.H. Abuwatfa, G.A. Husseini, Redox-responsive drug delivery systems: a chemical perspective, Nanomaterials 12 (2022) 3183.
38 E. Mauri, S.M. Giannitelli, M. Trombetta, A. Rainer, Synthesis of nanogels: Current trends and future outlook, Gels 7 (2021) 36.
39 G. Yu, X. Chen, Host-guest chemistry in supramolecular theranostics, Theranostics 9 (2019) 3041.
40 M. Nakahata, Y. Takashima, H. Yamaguchi, A. Harada, Redox-responsive selfhealing materials formed from host–guest polymers, Nat. Commun. 2 (2011) 511.

41 G. Sinawang, M. Osaki, Y. Takashima, H. Yamaguchi, A. Harada, Supramolecular self-healing materials from non-covalent cross-linking host–guest interactions, Chem. Commun. 56 (2020) 4381–4395.
42 A. Sugawara, T.-A. Asoh, Y. Takashima, A. Harada, H. Uyama, Mechano responsive hydrogels driven by the dissociation of a host–guest complex, ACS Macro Lett. 10 (2021) 971–977.
43 A. Hashidzume, H. Yamaguchi, A. Harada, Cyclodextrin-based rotaxanes: from rotaxanes to polyrotaxanes and further to functional materials, Eur. J. Org. Chem. 2019 (2019) 3344–3357.
44 M. Adeli, M. Kalantari, Z. Zarnega, R. Kabiri, Cyclodextrin-based dendritic supramolecules; new multivalent nanocarriers, RSC Adv. 2 (2012) 2756–2758.
45 A. Siekierka, K. Smolińska-Kempisty, J. Wolska, Enhanced specific mechanism of separation by polymeric membrane modification—A short review, Membranes 11 (2021) 942.
46 M. Giulbudagian, S. Hönzke, J. Bergueiro, D. Işık, F. Schumacher, S. Saeidpour, S. Lohan, M. Meinke, C. Teutloff, M. Schäfer-Korting, Enhanced topical delivery of dexamethasone by β-cyclodextrin decorated thermoresponsive nanogels, Nanoscale 10 (2018) 469–479.
47 N.K. Verma, A. Sadeer, A. Kizhakeyil, J.H. Pang, Q.Y.A. Chiu, S.W. Tay, P. Kumar, S. A. Pullarkat, Screening of ferrocenyl–phosphines identifies a gold-coordinated derivative as a novel anticancer agent for hematological malignancies, RSC Adv. 8 (2018) 28960–28968.
48 Q. Ling, F. Zhen, D. Astruc, H. Gu, ROMP synthesis of side-chain ferrocenecontaining polyelectrolyte and its redox-responsive hydrogels showing dramatically improved swelling with β-cyclodextrin, Macromol. Rapid Commun. 42 (2021) 2100049.
49 J. Woo, Y. Na, W.I. Choi, S. Kim, J. Kim, J. Hong, D. Sung, Functional ferrocene polymer multilayer coatings for implantable medical devices: Biocompatible, antifouling, and ROS-sensitive controlled release of therapeutic drugs, Acta Biomater. 125 (2021) 242–252.
50 K. Hande, Etoposide: Four decades of development of a topoisomerase II inhibitor, Eur. J. Cancer 34 (1998) 1514–1521.
51 M.H. Jouybari, S. Hosseini, K. Mahboobnia, L.A. Boloursaz, M. Moradi, M. Irani, Simultaneous controlled release of 5-FU, DOX and PTX from chitosan/PLA/5-FU/gC3N4-DOX/g-C3N4-PTX triaxial nanofibers for breast cancer treatment in vitro, Colloids Surf. B Biointerfaces 179 (2019) 495–504.
52 J. Gao, Z. Chen, X. Li, M. Yang, J. Lv, H. Li, Z. Yuan, Chemiluminescence in combination with organic photosensitizers: beyond the light penetration depth limit of photodynamic therapy, Int. J. Mol. Sci. 23 (2022) 12556.
53 S. Saraf, M.K. Gupta, Itraconazole loaded ethosomal gel system for efficient treatment of skin cancer, Int. J. Drug Deliv. 10 (2018) 12–19.
54 S.M. Querobino, N.C. de Faria, A.A. Vigato, B.G. da Silva, I.P. Machado, M.S. Costa, F.N. Costa, D.R. de Araujo, C. Alberto-Silva, Sodium alginate in oil-poloxamer organogels for intravaginal drug delivery: Influence on structural parameters, drug release mechanisms, cytotoxicity and in vitro antifungal activity, Mater. Sci. Eng. C. 99 (2019) 1350–1361.
55 S. Zhang, Y. Gu, Z. Shi, N. Lu, H. Xu, A novel reversible fluorescent probe based on naphthalimide for sequential detection of aluminum (Al3+) and fluoride (F−) ions and its applications, Anal. Methods 13 (2021) 5360–5368.
56 Y. An, T. Jin, F. Zhang, P. He, Electric cell-substrate impedance sensing (ECIS) for profiling cytotoxicity of cigarette smoke, J. Electroanal. Chem. 834 (2019) 180–186.
57 S. Liao, M. Zhao, J. Luo, K. Luo, J. Wu, R. Liu, S. Wang, P. Jia, Y. Bai, X. Zheng, The interaction mechanism between alkaloids and pepsin based on lum-AuNPs in the chemiluminescence analysis, RSC Adv. 9 (2019) 25569–25575.
58 C. Chun, S.M. Lee, C.W. Kim, K.-Y. Hong, S.Y. Kim, H.K. Yang, S.-C. Song, Doxorubicin–polyphosphazene conjugate hydrogels for locally controlled delivery of cancer therapeutics, Biomaterials 30 (2009) 4752–4762.
59 F. Zhao, A. Dong, L. Deng, R. Guo, J. Zhang, Morphology control and property design of boronate dynamic nanostructures, Polym. Chem. 10 (2019) 2436–2446.
60 B. Seiwert, U. Karst, Ferrocene-based derivatization in analytical chemistry, Anal. Bioanal. Chem. 390 (2008) 181–200.
61 Y. Sato, S. Yabuki, F. Mizutani, Electrochemiluminescence of luminol generated at self-assembled monolayer of ferrocenylalkanethiol on gold electrode, Chem. Lett. 29 (2000) 1330–1331.
62 X. Wang, X. He, Z. He, L. Hou, C. Ge, L. Wang, S. Li, Y. Xu, Detection of prostate specific antigen in whole blood by microfluidic chip integrated with dielectrophoretic separation and electrochemical sensing, Biosens. Bioelectron. 204 (2022), 114057.
63 W. Liu, W. Cao, W. Liu, K. Du, P. Gong, Determination of phenol by flow-injection with chemiluminescence detection based on the hemin-catalysed luminol– hydrogen peroxide reaction, Spectrochim. Acta Part A Mol. Biomol. Spectrosc. 85 (2012) 283–287.
64 Y. Liu, Z. Liu, Y. Shi, Sensitive determination of epinephrine in pharmaceutical preparation by flow injection coupled with chemiluminescence detection and mechanism study, Luminescence 26 (2011) 59–64.
65 B.H. Hussein, Spectroscopic studies of 7, 8-dihydroxy-4-methylcoumarin and its interaction with bovine serum albumin, J. Lumin. 131 (2011) 900–908.
66 M.V.N. Raj, K. Bhar, S. Jain, M. Rana, T.A. Khan, A.K. Sharma, Syntheses, X-ray structures, electrochemical properties and biological evaluation of mono-and dinuclear N2O2-donor ligand-Fe systems, Transit. Met. Chem. 44 (2019) 615–626.
67 V. Kolivoška, M. Gál, M. Hromadová, M. Valášek, L. Pospíšil, Correlation of the formation constant of ferrocene–cyclodextrin complexes with dielectric properties of the aqueous DMSO, Solut. J. Organomet. Chem. 696 (2011) 1404–1408.
68 R. Namgung, Mi Lee, Y. Kim, J. Jang, Y. Lee, B.-H. Kim, I.-S. Sokkar, P. Rhee, Y. M. Hoffman, A.S. Kim, W.J. Poly-cyclodextrin and poly-paclitaxel nano-assembly for anticancer therapy, Nat. Commun. 5 (2014) 3702.
69 Y. Xue, Y. Gao, F. Meng, L. Luo, Recent progress of nanotechnology-based theranostic systems in cancer treatments, Cancer Biol. Med. 18 (2021) 336.
70 V. Gutiérrez, A.B. Seabra, R.M. Reguera, J. Khandare, M. Calderón, New approaches from nanomedicine for treating leishmaniasis, Chem. Soc. Rev. 45 (2016) 152–168.
71 A. Giussani, P. Farahani, D. Martínez-Muñoz, M. Lundberg, R. Lindh, D. RocaSanjuán, Molecular basis of the chemiluminescence mechanism of luminol, Chem. A Eur. J. 25 (2019) 5202–5213.
72 R. Hatamvand, M. Adeli, A. Yari, Synthesis of glycerol-thiophene nanoparticles, a suitable sensing platform for voltammetric determination of guaifenesin, J. Polym. Sci. 58 (2020) 2784–2791.
73 R. Hatamvand, A. Shams, E. Mohammadifar, A. Yari, M. Adeli, Synthesis of boronic acid-functionalized poly (glycerol-oligoγ-butyrolactone): Nano-networks for efficient electrochemical sensing of biosystems, J. Polym. Sci. Part A Polym. Chem. 57 (2019) 1430–1439.
74 J.C. Cuggino, E.R.O. Blanco, L.M. Gugliotta, C.I.A. Igarzabal, M. Calderon, Crossing biological barriers with nanogels to improve drug delivery performance, J. Control. Release 307 (2019) 221–246.
75 M. Mohamadhoseini, Z. Mohamadnia, Supramolecular self-healing materials via host-guest strategy between cyclodextrin and specific types of guest molecules, Coord. Chem. Rev. 432 (2021), 213711.
76 S.B. Khan, S.-L. Lee, Supramolecular chemistry: Host–guest molecular complexes, Molecules 26 (2021) 3995.
77 Z. Zohreband, M. Adeli, A. Zebardasti, Self-healable and flexible supramolecular gelatin/MoS2 hydrogels with molecular recognition properties, Int. J. Biol. Macromol. 182 (2021) 2048–2055.
78 E. Bustos, J. Manríquez, E. Juaristi, T.W. Chapman, L.A. Godínez, Electrochemical study of β-Cyclodextrin binding with ferrocene tethered onto a gold surface via PAMAM dendrimers, J. Braz. Chem. Soc. 19 (2008) 1010–1016.
79 M. Dervisevic, M. Senel, T. Sagir, S. Isik, Highly sensitive detection of cancer cells with an electrochemical cytosensor based on boronic acid functional polythiophene, Biosens. Bioelectron. 90 (2017) 6–12.
80 Y. Liu, M. Wang, W. Liu, J. Jing, H. Ma, Olaparib and Doxorubicin Co-Loaded Polypeptide Nanogel for Enhanced Breast Cancer Therapy, Front. Bioeng. Biotechnol. 10 (2022), 904344.
81 A. Maruf, M. Milewska, A. Lalik, I. Wandzik, pH and reduction dual-responsive nanogels as smart nanocarriers to resist doxorubicin aggregation, Molecules 27 (2022) 5983.
82 Y. Wei, Y. Liu, Y. He, Y. Wang, Mitochondria and lysosome-targetable fluorescent probes for hydrogen peroxide, J. Mater. Chem. B 9 (2021) 908–920.
83 Y. Wu, T. Guo, Y. Qiu, Y. Lin, Y. Yao, W. Lian, L. Lin, J. Song, H. Yang, An inorganic prodrug, tellurium nanowires with enhanced ROS generation and GSH depletion for selective cancer therapy, Chem. Sci. 10 (2019) 7068–7075.
84 Y. Na, J.S. Lee, J. Woo, S. Ahn, E. Lee, W.I. Choi, D. Sung, Reactive oxygen species (ROS)-responsive ferrocene-polymer-based nanoparticles for controlled release of drugs, J. Mater. Chem. B 8 (2020) 1906–1913.